Kinetic consequences of the endogenous ligand to molybdenum in the DMSO reductase family: a case study with periplasmic nitrate reductase

Breeanna Mintmier[1], Jennifer M. McGarry[1], Daniel J. Bain[2], and Partha Basu[1]*

[1]Department of Chemistry and Chemical Biology, Indiana University-Purdue University Indianapolis

[2]Department of Geology and Environmental Science, University of Pittsburgh

*corresponding author: Partha Basu
Address: Department of Chemistry and Chemical Biology, Indiana University-Purdue University Indianapolis, 402 N Blackford St, Indianapolis IN 46202, USA.
Phone: 317 274 8935
Fax: 317 274 4701
Email: basup@iupui.edu

This is the author's manuscript of the article published in final edited form as:

Mintmier, B., McGarry, J. M., Bain, D. J., & Basu, P. (2021). Kinetic consequences of the endogenous ligand to molybdenum in the DMSO reductase family: A case study with periplasmic nitrate reductase. JBIC Journal of Biological Inorganic Chemistry, 26(1), 13–28. https://doi.org/10.1007/s00775-020-01833-9

Abstract

The molybdopterin enzyme family catalyzes a variety of substrates and plays a critical role in the cycling of carbon, nitrogen, arsenic, and selenium. The dimethyl sulfoxide reductase (DMSOR) subfamily is the most diverse family of molybdopterin enzymes and the members of this family catalyze a myriad of reactions that are important in microbial life processes. Enzymes in the DMSOR family can transform multiple substrates, however, quantitative information about the substrate preference is sparse, and, more importantly, the reasons for the substrate selectivity are not clear. Molybdenum coordination has long been proposed to impact the catalytic activity of the enzyme. Specifically, the molybdenum coordinating residue may tune substrate preference. As such, molybdopterin enzyme periplasmic nitrate reductase (Nap) is utilized as a vehicle to understand the substrate preference and delineate the kinetic underpinning of the differences imposed by exchanging the molybdenum ligands. To this end, NapA from *Campylobacter jejuni* has been heterologously overexpressed, and a series of variants, where the molybdenum coordinating cysteine has been replaced with another amino acid, has been produced. The kinetic properties of these variants are discussed and compared with those of the native enzyme, providing quantitative information to understand the function of the molybdenum coordinating residue.

Introduction

Molybdopterin containing enzymes have been contributing to life for millennia, dating as far back as 3.5–3.8 billion years. Furthermore, the molybdenum cofactor (Moco), the cofactor coordinating organic molybdopterin to molybdenum, was determined to be present in LUCA, the last universal common ancestor (1-3). Today there are over 50 different molybdopterin enzymes known to catalyze a variety of chemistries in the cycling of C, N, S, As, and Se, all relying on the same basic cofactor, the Moco (Figure 1A). The biochemical efficacy among the molybdopterin enzymes depends on the variations in the enzyme structure, particularly on the molybdenum coordination environments. However, the extent to which the structural variation impacts the kinetic proficiency remains unclear.

The extensive array of respiratory enzymes encoded by bacterial genomes enables a diverse metabolism. Of these respiratory enzymes, members of the DMSOR family such as nitrate reductase (NR), dimethyl sulfoxide reductase (DMSOR), trimethylamine N-oxide reductase (TMAOR), and formate dehydrogenase (FDH), contribute to this broad diversity. Many enzymes in the DMSOR family use oxygen atom transfer (OAT) reactions for substrate transformation, e.g. periplasmic nitrate reductase (Nap) and respiratory nitrate reductase (Nar) reduce nitrate to nitrite, TMAOR reduces TMAO to TMA, and DMSOR reduces DMSO to DMS.

The basic structure of Moco is depicted in Figure 1A, where the trigonal prismatic molybdenum center in DMSOR family members is coordinated by four sulfur donors from two molybdopterin (MPT) cofactors. The 5^{th} and 6^{th} positions vary depending on the enzyme (Figure 1). The 5^{th} position (Y in Figure 1A) is occupied by a coordinated amino acid residue and the 6^{th} position is defined as the terminal position (X in Figure 1). Thus,

the DMSOR family of enzymes has diverse active sites that vary in the first coordination sphere of the molybdenum center (Figure 1B). Interestingly, enzymes that catalyze the same reaction, such as Nap and Nar, have different molybdenum coordination spheres. In NapA, for instance, molybdenum is coordinated by a cysteine residue in the 5th position and an oxo or a sulfido group in the 6th position while in NarG the 5th position is held by an aspartate residue and the 6th position is an oxo group. Despite the variations at the molybdenum center, both NapA and NarG enzymes can reduce nitrate to nitrite (Figure 1B).

The coordinating residue has been hypothesized to tune the substrate preference through adjustments of physical properties of the molybdenum center (4). Expression of functional MPT enzymes has been challenging (5), nevertheless, progress in this area has been made (5-20). These pursuits have revealed that the coordinating residue is critical in the physiological function of the DMSOR family of enzymes while not required for Moco insertion and stability (9).

The substrate profiles of these enzymes have been limited to the natural substrates of the native enzyme. The consequences of exchanging the coordinating amino acid with respect to substrate selectivity of various substrates have not been fully explored. Thus, the mode of action of the coordinating residue in this family of enzymes is not completely understood. Herein, we examine the role of the coordinating residue through a kinetic and energetic perspective. The goal of this work is to develop a fundamental understanding of the extent that perturbations at the molybdenum center, specifically the coordinating amino acid residue, influence the function of members of the DMSOR family. To this end, we have selected periplasmic nitrate reductase (NapA) from *Campylobacter jejuni* (21)

as a model system. In this study alanine, serine, and aspartate variants of the coordinating cysteine in *C. jejuni* NapA have been produced and analyzed. Steady-state kinetic profiles for nitrate, TMAO, and DMSO activities for each variant have been determined to develop a quantitative picture. The data are presented and discussed in the context of the current knowledge of how molybdenum coordination influences the activity of the DMSOR family of enzymes.

Materials and Methods

Bacterial strains, plasmids, media, and growth conditions

Plasmids and oligonucleotides are listed in Table S1 (supplementary material). As previously described (21), *Escherichia coli* K12 (New England Biolabs Shuffle T7 *lysY* #C3027) cells containing the pBM10C plasmid were maintained on LB medium supplemented with 30 µg/mL kanamycin. Inoculated cultures were grown overnight at 37˚C, then transferred to 1 L of fresh autoinduction medium containing 12 g/L peptone, 24 g/L yeast extract, 1 g/L glucose, 2 g/L lactose, 0.50% (v/v) glycerol, and 90 mM potassium phosphate buffer pH 7.00. The cultures were supplemented with kanamycin (30 µg/mL), and Na_2MoO_4 (1 mM), then incubated at room temperature for 48 hours.

Site-Directed Mutagenesis

Mutagenesis of *C. jejuni napA* was conducted using the QuikChange II Site-Directed Mutagenesis Kit (Qiagen) with the pBM10C plasmid as a template as previously described (21). The primers designed for the *napA-C176S/A/D* mutations are listed in Table S1. The PCR product was sequenced at ACGT Inc. Plasmids pBM10C_C176S

(21), pBM10C_C176D, and pBM10C_C176A were expressed to produce the C176S, C176D, and C176A NapA variants, respectively.

Production and Purification of Recombinant Proteins

NapA (~108 kDa) and its variants were expressed and purified as previously described (21). Briefly, the cell pellets were resuspended in ice-cold buffer containing 50 mM HEPES, 300 mM sodium chloride, and 10 mM imidazole at pH 7.00. Cells were lysed by ultrasonication and the lysate was centrifuged at 7100 x g for 1 hour at 4°C. The crude enzyme was purified by immobilized metal ion affinity chromatography (HisTrap HP, GE Life Sciences), and size exclusion chromatography (HiPrep 16/60 Sephacryl S-200, GE Healthcare). The resulting NapA fractions were pooled, concentrated, and stored in buffer containing 50 mM HEPES pH 7.00 in liquid nitrogen. SDS-PAGE was used to screen fractions for NapA content and purity using standard protocols.

Steady-State Kinetics

Nitrate, TMAO, and DMSO reductase activities were measured spectrophotometrically by monitoring the oxidation of reduced methyl viologen at 600 nm as previously described (21). Assays under steady-state conditions were conducted in an inert atmosphere glove box at 25°C using a Bio-Tek Epoch2 Absorbance Microplate Reader. Assays were conducted with a total reaction volume of 250 µL (NapA) or 100 µL (variants). The addition of the substrate initiated the reaction which was monitored for 5 minutes (NapA) or 15 min (variants). The rate of methyl viologen oxidation was corrected by a blank measurement consisting of all reaction components except the substrate. Calculations were conducted using the Beer-Lambert law given the extinction coefficient of reduced methyl viologen (11,407 M^{-1} cm^{-1} at 600 nm). These rates were analyzed with

a non-linear Michaelis–Menten model using OriginPro 9 (OriginLab Inc.). For each measurement, three technical replicates were performed, and the concentration of the enzyme was corrected for the metal contents.

For pH experiments, methyl viologen was prepared as previously described (21) in the appropriate pH except for pH 5.5. NapA was pre-reduced by treatment with the appropriate pH methyl viologen solution for approximately 30-60 minutes (pH 5.5 was pre-reduced with pH 6.0 methyl viologen). The enzyme was further buffer exchanged in the appropriate pH buffer. The substrate was also diluted in the proper pH buffer. Assays were conducted with a total reaction volume of 250 µL (NapA) or 100 µL (variants). The reaction was initiated, monitored, and analyzed as described above. The reaction mixture's pH was tested to confirm a minimal shift in pH.

Protein Concentration Determination and Metal Analysis

Protein concentrations were determined using the Coomassie Plus (Bradford) Protein Assay Kit (Thermo Scientific) with bovine serum albumin as a standard (Pierce). Protein samples were analyzed for metal content as previously described (21).

Incremental Binding Energy Calculations

The incremental or change in the binding energy ($\Delta\Delta G_b$) of the enzyme and substrate as well as the incremental or change in binding energy ($\Delta\Delta G_b^{\ddagger}$) of the enzyme and transition state (22) were calculated using the kinetic parameters of the C176 NapA variants with equations (1) and (2).

$$\Delta\Delta G_b = -RT \ln\left(\frac{\left[{}^{1}/_{K_M}\right]_A}{\left[{}^{1}/_{K_M}\right]_B}\right) \quad (1)$$

$$\Delta\Delta G_b^{\ddagger} = -RT \ln\left(\frac{\left[{}^{k_{cat}}/_{K_M}\right]_A}{\left[{}^{k_{cat}}/_{K_M}\right]_B}\right) \quad (2)$$

The R represents the gas constant and T is the temperature in Kelvin. The term $(k_{cat}/K_M)_{A/B}$ represents the specificity constant under conditions A and B, respectively, while $(1/K_M)_{A/B}$ estimates the association constant of enzyme and substrate under conditions A and B, respectively. Two sets of conditions were analyzed to determine the $\Delta\Delta G_b$ and the $\Delta\Delta G_b^{\ddagger}$. The effect of the mutation while keeping the substrate (i.e., nitrate and TMAO) constant is represented in the first set of conditions. The second set of conditions represent the different substrates for the same variant; and all three variants were analyzed.

Determination of Essential pK_a Values

Analysis of the pH data was conducted utilizing the methods of Dixon (23,24) and Fersht (22) where the kinetic rate parameters are derived as a function of $[H^+]$ and the dissociation constants of protonation forms (K_a). The data for the native NapA were fit to equation (3), where k_{obs} is the observed kinetic parameter over the examined

$$\log(k_{obs}) = \frac{k_{max}}{1+10^{(pH-pK_1)}+10^{(pK_2-pH)}} \quad (3)$$

pH range, k_{max} is the pH corrected theoretical maximal value of the kinetic parameter being fit, and pK_1 and pK_2 are relevant pK_a values being fit.

Results

Variants of NapA and their Characterization

The Mo-coordinating residue in *C. jejuni* NapA, Cys176, has been successfully exchanged for Ser, Asp, and Ala as confirmed by DNA sequencing and LC-MS/MS has been used to confirm the C176S NapA variant (21). The Ser variant emulates the first coordination sphere of molybdenum in TMAO reductase (TMAOR), and DMSOR (Figure 1B). The Asp variant mimics the first molybdenum coordination sphere of NarG, while the Ala variant has been produced as a control where no amino acid residue is coordinated

to the Mo-center. Such a center has been found in arsenite oxidase (Aio) where molybdenum is not coordinated by a protein residue (Figure 1B) (25,26).

The purity of each protein preparation has been monitored by SDS-PAGE (Figure S1). The integrity of the [4Fe-4S] cluster has been observed by UV-Vis spectrometry with a band ~400 nm (Figure 2) similar to *Desulfovibrio desulfuricans* NapA (27) and cofactor incorporation has been measured via inductively coupled plasma mass spectrometry (ICP-MS) (Table S2). The Ser and Ala variants have reasonable molybdenum incorporation of 70-90% which is comparable to the native NapA enzyme (Table S2) while the Asp variant has significantly lower molybdenum incorporation. On average, the amount of holo C176D NapA variant isolated is 14-28 times lower than the yield of holoenzyme isolated for native NapA or the C176S/A NapA variants.

Steady-State Kinetics of NapA Variants using Nitrate as a Substrate.

Steady-state kinetic analysis of native NapA reveals an approximate K_M for nitrate of 3.4 μM and k_{cat} of 5.91 s^{-1} suggesting the enzyme has a high affinity for nitrate and is efficient at reducing nitrate as previously reported (21) (Table 1). Compared to the native NapA, the K_M in C176S NapA has increased 100-fold and k_{cat} has decreased by 2 orders of magnitude (Figure 3AB, Table 1). The C176D NapA variant shows attenuated nitrate reductase activity with a k_{cat} 17 times lower than the native NapA enzyme and a K_M for nitrate that is 1.5 times higher than the K_M for nitrate reduction by the C176S NapA variant (Figure 3C, Table 1). Unlike the C176S/D NapA variants, C176A NapA is inactive towards nitrate. Exchanging the sulfur donor from Cys for an oxygen donor from either Asp or Ser

decreases k_{cat} and increases K_M for nitrate reduction while the uncoordinated variant completely abolishes nitrate reductase activity.

TMAO and DMSO Reductase Activity

Both native NapA and C176S NapA reduce TMAO, with C176S NapA having a slightly higher k_{cat} for reduction of TMAO; both enzymes have similar k_{cat}/K_M for TMAO reduction. (Figure 4, Table 1) The K_M of native NapA increases by 50 times when nitrate is substituted with TMAO as the substrate, and the k_{cat} for nitrate is 64 times higher than the k_{cat} for TMAO. The opposite effect is observed for C176S NapA. Here, the K_M for C176S NapA with TMAO as substrate decreases by a factor of 1.5 compared to the K_M of nitrate for C176S NapA. The k_{cat} of C176S NapA for TMAO reduction increases 2-fold as compared to C176S NapA nitrate reduction k_{cat} (Table 1). Interestingly, C176D NapA does not reduce TMAO. DMSO reductase activity is nonexistent in native NapA as well as in C176S NapA, however, C176D NapA shows marginal activity (Figure 5, Table 1). The K_M of the C176D NapA for DMSO decreases 16.5 times and the k_{cat} decreases by ~15 times when compared to C176D NapA towards nitrate activity (Table 1). Unlike the C176S/D variants, C176A NapA is inactive toward nitrate, DMSO, and TMAO.

Incremental Binding Energy

Kinetic values have been used to approximate the incremental binding energy between two conditions (e.g., between two substrates, or mutational variants) to reveal useful information about energy states of the enzyme during substrate transformations (22). The pseudo second-order rate constant, k_{cat}/K_M, is used to determine the activation energy for nitrate reduction by NapA denoted as $\Delta G_T^{\ddagger}$. This energy value is composed of two terms. First, the energetically unfavorable term $\Delta G_0^{\ddagger}$, which represents the activation

energy of the chemical steps where bonds are broken and formed, determined from k_{cat}. The second term consists of the energetically favorable term ΔG_b, which represents the binding energy (e.g., from the K_D or estimated from K_M when S binds to E). As such, differences in these parameters induced by amino acid exchange or altering substrates provide information about the energetics of the reaction as a function of the mutation or substrate.

Transition state theory in combination with the enzymatic kinetic model (e.g., Michaelis-Menten) can be utilized for calculating $\Delta\Delta G_b$, the incremental or change in the binding energy of the enzyme and substrate as well as $\Delta\Delta G_b^{\ddagger}$ the incremental or change in the binding energy of the enzyme and transition state (22) as given in equations (1) and (2). For analysis of the NapA variants, two sets of conditions have been analyzed to determine the $\Delta\Delta G_b$ and the $\Delta\Delta G_b^{\ddagger}$ (Table 2). The effect of the mutation is represented in the first set and the second set represents the effect of different substrates for the same variant.

The $\Delta\Delta G_b$ and the $\Delta\Delta G_b^{\ddagger}$ values are listed in Table 2. The $\Delta\Delta G_b$ values represent the difference in the binding energy of the substrate and the enzyme variants. A negative $\Delta\Delta G_b$ value suggets, condition A lowers the energy level of the ES complex by $\Delta\Delta G_b$ than that of the ES complex under condition B. Similarly, the $\Delta\Delta G_b^{\ddagger}$ value represents the difference in the binding energy of the enzyme or its variants with the substrate in the transition state, [$ES^{\ddagger}$]. Thus, the change in binding energy reveals that the native NapA enzyme has a lower [$ES^{\ddagger}$] free energy with nitrate as substrate by approximately 23.2 kJ/mol ($\Delta\Delta G_b^{\ddagger}$) and 19.2 kJ/mol ($\Delta\Delta G_b^{\ddagger}$) than the C176S and C176D variants, respectively. Additionally, the native NapA enzyme has lower energy for the ES complex

by approximately 11 kJ/mol ($\Delta\Delta G_b$) and 12 kJ/mol ($\Delta\Delta G_b$) than the C176S and C176D variants, respectively. The patterns observed by these changes in binding energy are depicted in Figure 6A.

Similarly, the C176D NapA has a lower [ES‡] free energy than C176S NapA by ~4 kJ/mol ($\Delta\Delta G_b^{\ddagger}$) and a higher ES energy level by ~1 kJ/mol ($\Delta\Delta G_b$) (Figure 6B, Table 2). When comparing the impact of the Ser residue on TMAO activity, the native NapA has ~598 J/mol ($\Delta\Delta G_b$) lower energy for the ES state and ~178 J/mol ($\Delta\Delta G_b^{\ddagger}$) lower energy for the [ES‡] state compared to the C176S NapA variant with TMAO as substrate (Figure 6C, Table 2). Additionally, for the native NapA enzyme which can turn over both nitrate and TMAO, the energy for the reduction of nitrate for the ES state and the [ES‡] state, respectively, are ~9.5 kJ/mol ($\Delta\Delta G_b$) and ~19.8 kJ/mol ($\Delta\Delta G_b^{\ddagger}$) lower than that of reducing TMAO (Figure 6D, Table 2). Furthermore, C176S NapA has a ~3.1 kJ/mol ($\Delta\Delta G_b^{\ddagger}$) lower [ES‡] energy and ~1 kJ/mol ($\Delta\Delta G_b$) lower ES energy for TMAO versus nitrate reduction (Figure 6E, Table 2). Likewise, the C176D mutation lowers the ES and the [ES‡] energies for DMSO versus nitrate reduction by ~7 kJ/mol ($\Delta\Delta G_b$) and ~262 J/mol ($\Delta\Delta G_b^{\ddagger}$) respectively (Table 2, Figure 6F).

Nitrate Activity Dependence on pH

A pH profile of the nitrate reductase activity has been developed for all active variants. The pH optimum has been determined for *C. jejuni* NapA with a calculated maximum k_{cat} at pH 7.4 (Figure 7) while the maximum efficiency (k_{cat}/K_M) is observed at pH 7.0. The change in k_{cat} due to pH is small, a difference of ~6 s^{-1} between the pH where the enzyme is most active and that where the enzyme is least active. The impact on K_M displays no obvious pattern and the change in K_M ranges from 2.5 to 8.1 μM (Table S3).

Due to the inactivity of the C176A NapA variant, pH studies have not been performed. C176S NapA has a pH optimum at pH ~ 7.0 (Figure S2). The change in k_{cat} due to pH is small, shifting < 1 s^{-1} but still larger than the standard error (±0.009 s^{-1}) associated with k_{cat}. The K_M increases linearly, from 65 μM to 700 μM, over the pH range of 5.5-9.0 (Table S3). The C176D NapA variant has a pH optimum of ~6.3 (Figure S2). The K_M of C176D NapA increases with pH similar to C176S NapA. In addition, C176D NapA's k_{cat}/K_M decreases with increasing pH. The trends for all three of the kinetic parameters suggest C176D NapA prefers slightly acidic conditions for higher activity.

The pH data have been further analyzed to determine pK_a values that are essential for nitrate reductase activity in NapA. This approach has successfully been applied in understanding the pH effect in arylsulphatase (28) and SO (29). The native NapA pH data have been successfully fit to equation (3) where pK_a values were determined to be 5.44 and 9.38 (Figure 8A). However, the C176S/D NapA variants data as a function of pH (Figure 8B and 8C) cannot be fit with equation (3). Instead, the data have been fit with high order polynomials, which provide a means of analyzing them qualitatively (Figure 8B and 8C). The inflection points in the polynomials have been identified, and from these the pKa values of the ionization steps that diminish nitrate reduction rates are estimated to be between 6.6 and 7.7 for C176D NapA, and between 7.1 and 8.3 for C176S NapA.

Discussion

Alternative Substrates of the C176 NapA Variants

The natural substrate for NapA is nitrate and reduction of S or N-oxides by NapA has not been reported. DMSOR and TMAOR natural substrates are DMSO and TMAO,

respectively, where both enzymes have a Ser coordinated Mo-center (Figure 1B) (30). The present work shows both native *C. jejuni* NapA and C176S NapA can reduce TMAO. The K_M values are similar to *E. coli* TMAOR (Table 1) while the turnover is severely reduced. The TMAO reduction efficiencies of native NapA and C176S NapA are similar to one another (Figure 4, Table 1), while theC176D/A NapA variants, are completely inactive toward TMAO.

Neither the native NapA nor the C176S/A NapA variants could reduce DMSO, however, the C176D NapA variant is active towards DMSO albeit with a slow turnover rate (Figure 5, Table 1). This observation suggests that the Asp substitution is able to tune substrate specificity toward a previously inactive substrate. Similar results have been observed in *R. sphaeroides* DMSOR where both the native and the S147C variant can reduce adenosine-^{1}N-oxide (ANO), however, the activity is 400% higher in the variant (13). In the present case, the Asp ligand impacts the substrate affinity and/or the binding process. The K_M of DMSO is 28.2 μM compared to that of nitrate at 462 μM for C176D NapA suggesting the Asp residue may be stabilizing a DMSO bound form.

It is interesting that the native NapA enzyme can turn over TMAO but not DMSO. DMSO reductases can reduce both S and N-oxides while TMAO reductases are more selective, and can efficiently reduce N-oxides only (19). Kaufmann *et al*. (11) reports that a TMAOR variant where the molybdenum coordinating residue Ser is exchanged for a Cys has approximately 40% TMAO specific activity compared to the native TMAOR. Similarly, Hilton *et al*. (13) observes 21% TMAO specific activity in the *R. sphaeroides* S147C DMSOR variant. Consistent with the ability of native *C. jejuni* NapA to reduce TMAO, mutations of the coordinating Ser to Cys in TMAOR exhibit TMAOR activity.

Interestingly, Hilton *et al*. (13) observes 39% DMSO specific activity in the *R. sphaeroides* S147C DMSOR variant and thus, the inability of the native NapA to reduce DMSO is unexpected. The apparent discrepancy in substrate selectivity suggests additional factors may be in play.

According to Johnson *et al*. (19) the presence of a Tyr residue in *R. sphaeroides* DMSOR preferentially selects for S-oxides over N-oxides and this Tyr is absent in both *E. coli* TMAOR and Nap. The presence of Tyr114 in *R. sphaeroides* DMSOR increases the catalytic efficiency of DMSOR for S-oxides as compared to N-oxides (Figure 9). Insertion of a Tyr residue in TMAOR mimicking Tyr114 increases the efficiency of the TMAOR reduction of S-oxides (19). Ridge *et al*. (31) notes that the Tyr114 in *R. sphaeroides* DMSOR is in close proximity to the sulfur atom of the bound DMSO (~3.3 Å) which has led them to propose that the Tyr may have a role in weakening the S-O bond in bound DMSO through an interaction between the sulfur atom and the hydroxy side chain of Tyr.

Secondary structure matching (SSM) analysis (32) shows that in place of Tyr114 of DMSOR, Nap has Gly144. Without the stabilization of the intermediate provided by Tyr114 in DMSOR, NapA may be unable to tightly bind DMSO as would be necessary for catalysis. The single change of the Cys-S ligand to an Asp-O ligand may mimic DMSO stabilization by Try114 in C176D NapA via interaction with the carboxylate side chain of Asp (Scheme 1). Stabilization of this putative DMSO bound intermediate enables this variant to turnover DMSO. This aspect will be probed in the future to determine the exact nature of the mutation enabling DMSOR activity.

Implications of Mo Ligand Exchange in Energetics

The elementary steps involved in nitrate reduction by NapA are schematically shown in Scheme 2. In this scheme, as isolated enzyme in the oxo-Mo(VI) state, denoted as E^o, is reduced by two coupled electron proton transfer (CEPT) processes to generate the reactive Mo(IV) state (E). Under the assay conditions this process is accomplished by reduced methyl viologen. The substrate nitrate, denoted as S, binds to this E state forming the enzyme-substrate (ES) complex. In the transition state, [$ES^{‡}$], the enzyme forms a complex with S where the N-O bond is weakened and the Mo=O moiety begins to form (Scheme 2). Nitrite is released regenerating the oxo-Mo(VI) state, E^o.

It has been demonstrated that the electron transfer steps during the regeneration of the reduced Mo(IV) state from the oxidized Mo(VI) state of Nap enzymes are faster than the catalytic turnover (33,34) and thus are not rate-limiting. Therefore, in the present case, we have examined the energetics more globally rather than focusing on the effect of redox potentials due to the substitution of the coordinating residue which undoubtedly would impact the redox potentials of the molybdenum center. We specifically focus on the substrate transformation steps probing the energetics of the ES complex and [$ES^{‡}$] during the course of the reaction.

The impact of the Ser mutation on the energetics of nitrate reduction by NapA has been probed (Figure 6A). The differential energy changes in ES and [$ES^{‡}$] reveal an incongruent pattern where the mutation influences energies of both states to different extent. A similar pattern is observed for the nitrate reduction by the Asp mutation (Figure 6A). This result suggests the coordinating Cys residue is involved in nitrate reduction by stabilizing the ES and [$ES^{‡}$] states. A larger change in [$ES^{‡}$] than the ES state suggests

that the Mo coordinating residue impacts the energy of the transition state to a greater extent than substrate binding. The lower free energy of [$ES^{‡}$] for the native NapA compared with [$ES^{‡}$] for the C176S/D NapA variants, implies that theactivation energy for nitrate reduction is lower for the native enzyme.Interestingly, C176D NapA has a lower [$ES^{‡}$] free energy than C176S NapA suggesting the oxygen donor to the molybdenum center may not be the only factor influencing the driving force for reduction of nitrate.

Remarkably, the change in binding energy for the mutation of Ser on TMAO reduction is less significant than the previously mentioned binding energies with respect to nitrate reduction. As shown in Figure 6C, native NapA has a lower energies for ES and [$ES^{‡}$] states compared to C176S NapA with TMAO as substrate implying that the activation energies of these enzymes for the reduction of TMAO are very similar and leading to similar efficiencies. The energies of the [$ES^{‡}$] states are essentially the same resulting in a minimal change in activation energies consistent with the almost identical k_{cat} values for the two variants. Although both the [$ES^{‡}$] and the ES states are almost isoenergetic in two Nap variants, the larger energy differences are observed in the ES states. Such a result suggests that the Ser residue is impacting the binding energy by destabilizing the ES state. Thus, the destabilized ES state increases K_M which may result in a small increase in k_{cat}. As a result, the slightly higher increase in the native NapA TMAO reduction efficiency can be attributed to the lower ES binding energy and thus a lower K_M for the native NapA enzyme.

The impact of substrates for a particular variant on incremental binding energy has also been analyzed. For the native NapA enzyme, both the ES and [$ES^{‡}$] state energies are lower for the reduction of nitrate as compared to TMAO. The energy values suggest

that reduction of TMAO has a higher activation energy barrier than that of nitrate for the native NapA enzyme (Figure 6D). The binding energies of TMAO reduction by the native NapA and C176S NapA are very similar with a $\Delta\Delta G_b$ value of -598 J/mol and a $\Delta\Delta G_b^{\ddagger}$ of -178 J/mol suggesting there is a small difference in substrate specificity for C176S NapA. This observation is corroborated by lowering of [ES‡] and ES energies for TMAO versus nitrate reduction by C176S NapA (Figure 6E).

The change in the ES binding energy for C176S NapA from nitrate to TMAO is smaller than that in native NapA, where the native enzyme favors nitrate and the C176S variant favors TMAO. While the kinetic efficiencies reveal no impact of the Ser residue on TMAO turnover, the energy calculations indicate the Ser ligand tunes substrate selectivity. The substrate preference is adjusted by essentially lowering the activation energy barrier through destabilization of the ES and [ES‡] states of C176S NapA with nitrate instead of stabilizing the states in the reaction with TMAO. This result is supported by the fact that for the native NapA and the C176S NapA variant, TMAO energy states are similar. Likewise, the C176D mutation lowers the ES and the [ES‡] energies for DMSO versus nitrate reduction (Table 2, Figure 6F). The Asp mutation impacts the ES state to a greater degree supporting the previous hypothesis that the Asp ligand can stabilize the DMSO binding to the enzyme while the other variants cannot.

The Impact of pH on Nitrate Reduction Catalyzed by the C176 NapA Variants

The coordinating residue appears to impact binding and influences the stabilization of the ES and [ES‡] complexes thus impacting the driving force and kinetic rate of the reaction in order to tune substrate selectivity. The exact mechanism of action for this stabilization of ES and/or [ES‡] is unclear. In formate dehydrogenase, FDH, the

coordinating residue has been hypothesized to participate in the proton shuttling capability of the enzyme (4). Exchanging the coordinating residue could impact the proton shuttle pathway directly as seems to be the case for *E. coli* FDH where the SeCys is suggested to abstract the proton from formate after C-H bond cleavage (4). The coordinating amino acid could also have an indirect role, where it is possible that the pK_a of the catalytic pocket has been altered by exchanging coordinating residues. This situation could, in turn, impact the formation of the ES complex or the stabilization of the transition state, [$ES^{‡}$], thus altering the energetics of the enzyme and tuning substrate preference. The pH profiles of each nitrate active variant have been examined to explore the impact the coordinating residue may have on the pK_a of the residues forming the active site of Nap and possibly the proton shuttling process.

Interestingly, *C. jejuni* NapA's k_{cat} and K_M do not vary significantly with pH (Table S3, maximum shift in K_M is 6 μM and that for k_{cat} is 6 s^{-1}). While pH dependence has been reported for other Nap enzymes (17,35-38), the majority of reports present the data as percent activity of Nap at various pH conditions (35-37). As a result, comparing the pH effect on kinetic parameters is difficult. However, a recent study on *R. sphaeroides* Nap reports the pH dependence of both K_M and k_{cat} over a pH range of 5.0-8.0 (38). Zeamari *et al.* (38) observes a change in K_M of 50 μM to 250 μM, which is significantly different than that of the *C. jejuni* NapA value of ~6 μM. Furthermore, Zeamari *et al*. (38) reports a change in k_{cat} of ~50 s^{-1} as compared to the 6 s^{-1} difference in *C. jejuni* NapA. Interestingly, *R. sphaeroides* is a free-living microbe often found in soil or aquatic environments (39). Perhaps the insensitivity to pH observed in *C. jejuni* NapA is, in part, aiding in the virulence of the pathogen as compared to the free-living microbe, *R. sphaeroides*. In fact,

pH has been reported to impact the expression of several virulence factors, and pH conditions significantly impact biofilm formation, a common factor that prevents the efficient treatment of several pathogens (40-44). Perhaps the general resistance to pH changes observed in *C. jejuni* NapA contribute to the pathogen's virulence. The pH resistance may also be a mechanism to confront the physiological pH equilibria in the GIT of the hosts that *C. jejuni* tends to colonize.

The C176S and C176D NapA variants have similar pH optima of 7.0 and 6.3, respectively (Figure S2). The most notable feature of these pH profiles is the impact that the coordinating residue seems to have on K_M and effectively on substrate affinity. The K_M of both variants increases with more alkaline pH while no obvious pattern is observed for the native NapA's K_M value over the same pH range (Figure S2, Table S3). The data suggest that the oxygen donor provided by both Ser and Asp ligands impacts the pK_a of the Nap active site and is influencing the protonation state of residues that stabilize substrate binding. The differential pH effect of the variants compared to the native enzyme may explain the difference in (de)stabilization of the ES and [$ES^{‡}$] states by the exchanged coordinating residues.

The double logarithm plot of $\log(k_{cat})$ as a function of pH (as in equation (3)) for native NapA (Figure 8A) where k_{cat} is equal to k_2 in the enzyme equations in Scheme 3A reveals information on the ionization of only the ES complex. As such, there are two possible ionizations in the ES complex that impact catalysis. The first pK_a represents an ionization where the deprotonated form is necessary for activity. The second pK_a represents ionization of a separate entity where deprotonation inactivates the enzyme and thus the protonated form of this residue is necessary for optimal activity. Hence,

equation (3) assumes the single protonated form (EHS^-) is the only catalytically active form (Scheme 3A). The pK_a of 5.44 represents the residue in the enzyme that is catalytically important in its deprotonated form. This residue could be an Asp or Glu whose usual pK_a range is 2-5.5 in proteins or it could be a His, which has a pk_a range of 5-8 (22).

According to a homology model of *C. jejuni* NapA (21), there are no Asp or Glu residues within hydrogen bonding distance to the molybdenum center. The other possible residue the pK_a of 5.44 could represent is a His residue. There are two His residues in close proximity to the molybdenum center. Residue H822 is positioned slightly under the molybdenum center in between the two MPT molecules and thought to interact in the hydrogen bonding network of the MPT molecules. Residue H175 is directly next to the coordinating C176 residue and positioned above the molybdenum center in the catalytic pocket. Effects of both His175 and His822, in NapA will be investigated with additional mutagenesis studies in the future. The second pK_a of 9.38 represents the deprotonation of a residue that inactivates the enzyme. This residue could be a Tyr which usually has a pK_a range of 9-12 or it could be a Cys which has a pk_a range of 8-11 (22). Further investigation is needed to test these possibilities.

The C176S/D NapA variants exhibit a more complicated profile as the plots of $\log(k_{cat})$ as a function of pH (Figure 8B and C) cannot be fit with equation (3). The data have been fit to high order polynomials and the shape of the fit suggests that two protonic states (EHS^- and ES^{2-}) can yield products as shown in Scheme 3B (24). The observation of the higher of the two maxima at low pH compared to the lower of the two maxima at high pH (Figure 8B and C) further suggests the deprotonation diminishes the rate of nitrate reduction and further deprotonation may even inactivate the enzyme (24). The

difference in the two maxima is larger in C176S NapA (Figure 8B) suggesting the diminishing rate effect on catalysis at higher pH may be more significant in this variant which is supported by the kinetic data where k_{cat} for C176S NapA at optimal pH is 0.159 s^{-1} and k_{cat} for C176D NapA at optimal pH is 0.530 s^{-1} (Table S3).

Through determination of the inflection points of the polynomial fits (Figure 8B and C), we can estimate that the pK_a for the ionization step that diminishes the rate of nitrate reduction may be between 6.6 and 7.7 for C176D NapA and between 7.1 and 8.3 for C176S NapA. However, the pK_a estimates are inexact for complex ionization patterns especially when multiple pK_a values are close together as they are in this case. The main result of the pH profile of the coordinating residue variants indicates that the coordinating residue does impact key ionizations during catalysis. It is tempting to suggest that the change in protonation states and proton shuttling in the C176 Nap variants may cause the energetic changes discussed above. However, further investigation is needed to confirm how the mutation is impacting pK_a and which partner residues in the pocket are affected.

Summary

DMSOR family enzymes can transform different substrates and the coordinated amino acid residues influence the enzyme efficiency as well as the substrate affinity. The Asp variant of Nap is reported for the first time. This is the first investigation into the TMAO and DMSO activities of any Nap variants and is also the first documentation of TMAOR activity by a Nap enzyme. Remarkably, the C176D NapA variant reduces DMSO but not TMAO, whereas the other variants can only reduce TMAO. This investigation represents a detailed kinetic and energetic perspective of the molybdenum coordinating residues.

Analysis of the incremental binding energies of the ES and [ES‡] states of the Nap C176 variants suggests. Determination of the binding energies suggest:

- The coordinating Cys residue is involved in stabilizing the ES and more significantly the [$ES^{‡}$] states during the catalysis of nitrate reduction.
- The activation energy for nitrate reduction is lower for the native NapA compared to the C176S/D NapA variants.
- The coordinated Ser residue impacts the binding energy by destabilizing the ES state in TMAO reduction and thus increasing K_M compared to native NapA that results in a small increase in k_{cat}. Consequently, the slightly higher increase in the native enzyme's TMAO reduction efficiency can be attributed to the lowering of the ES binding energy and lowering of K_M in native NapA.
- TMAO reduction has a higher activation energy barrier than nitrate reduction for native NapA.
- The Ser ligand does indeed tune substrate selectivity by essentially lowering the activation energy barrier by destabilizing the ES and [$ES^{‡}$] states of C176S NapA and nitrate instead of stabilizing the states in the reaction with TMAO.
- The Asp mutation impacts the ES state to a greater degree than the [$ES^{‡}$] which supports the hypothesis that the Asp ligand can stabilize the DMSO binding to the enzyme when the other variants cannot.

Additionally, the pH profiles of the C176 variants have been investigated to see if the differences in energetics and kinetics are related to proton shuttling. The insensitivity to pH observed in *C. jejuni* NapA may in part be aiding in the virulence of the pathogen as compared to free-living microbes. Native NapA, C176S NapA, and C176D NapA have pH

optima at 7.4, 7.0, 6.3 respectively but the most notable feature of these pH profiles is the impact the coordinating residue seems to have on K_M and effectively on substrate affinity. The K_M of both C176S/D variants increases with more alkaline pH while no obvious pattern is observed for the native NapA's K_M value over the same pH range. The main finding of the pH profile of the coordinating residue variants indicates that the coordinating residue does impact key ionizations during catalysis.

Under the assumption that the majority of the DMSOR family follow OAT reaction as the *modus operandi* regardless of the substrate, then the differences lie in nature's way of selecting the most efficient conditions to turn over a specific substrate. The coordinating residue is one component that nature has utilized to accomplish this goal to tune substrate selectivity as highlighted by the efficiencies of the TMAO and DMSO activity of these Nap variants. A quantum mechanics/molecular mechanics (QM/MM) study is ongoing in our laboratory that will further address how the various mutations structurally perturb the structure of *C. jejuni* NapA. Specifically, focusing on the dynamics of the variants that may contribute to the kinetic and energetic results reported here.

Data Availability

The authors have included all data sets in the manuscript or in the supporting information. Additional details may be provided upon request to the corresponding author.

Acknowledgments

The authors would like to acknowledge Professor Russ Hille and Dr. Alexander Latta for helpful discussions. The authors greatly appreciate instrumental assistance from Professor Michael McLeish.

Funding and Additional Information

The authors would like to acknowledge the IUPUI School of Science and the National Science Foundation (CHE 2003752) for partial financial support of this work.

Conflicts of Interest

The authors declare that they have no conflicts of interest with the contents of this article.

Table 1: Kinetic parameters of *C. jejuni* NapA and its variants compared to similar DMSOR family enzymes

Enzyme[a]	Substrate	K_m (μM)	k_{cat} (s^{-1})	k_{cat}/K_m (1/s*M)	Reference
Cj native NapA	Nitrate	3.4 ± 0.44	5.91 ± 0.176	1.74×10^6	(21)
Cj C176S NapA	Nitrate	307 ± 16	0.045 ± 0.001	1.47×10^2	(21)
Cj C176D NapA	Nitrate	462 ± 66	0.339 ± 0.012	7.34×10^2	This work
Cj C176A NapA	Nitrate	*Inactive*	*Inactive*	*Inactive*	This work
Cj native NapA	TMAO	161 ± 20	0.092 ± 0.0026	5.71×10^2	This work
Cj C176S NapA	TMAO	205 ± 7	0.109 ± 0.0015	5.33×10^2	This work
Cj C176D NapA	TMAO	*Inactive*	*Inactive*	*Inactive*	This work
Cj C176A NapA	TMAO	*Inactive*	*Inactive*	*Inactive*	This work
Cj native NapA	DMSO	*Inactive*	*Inactive*	*Inactive*	This work
Cj C176S NapA	DMSO	*Inactive*	*Inactive*	*Inactive*	This work
Cj C176D NapA	DMSO	28.2 ± 4.5	0.023 ± 0.001	8.16×10^2	This work
Cj C176A NapA	DMSO	*Inactive*	*Inactive*	*Inactive*	This work
Rs NapAB	Nitrate	120	70.2	5.9×10^5	(18)
Pp NapAB	Nitrate	112	58	5.2×10^5	(45)
Ec TMAOR	TMAO	210 ± 100	2500 ± 200	1.2×10^7	(19)
Rs DMSOR	DMSO	7 ± 1	50 ± 2	7.1×10^6	(19)
Ec NarG	Nitrate	2	7.2	3.63×10^6	(20)

[a]*Cj-Campylobacter jejuni, Rs- Rhodobacter sphaeroides, Pp- Paracoccus pantotrophus, Ec-Escherichia coli*

Table 2: Calculated $\Delta\Delta G_b$ and $\Delta\Delta G_b^{\ddagger}$ values highlighting the effects of mutation and substrate for the enzyme-substrate complex and for the enzyme bound transition state of the *C. jejuni* NapA variants.

Enzyme A[a]	Substrate A[a]	Enzyme B[b]	Substrate B[b]	$\Delta\Delta G_b$ (J/mol)[c]	$\Delta\Delta G_b^{\ddagger}$ (J/mol)[d]
Native NapA	Nitrate	C176S NapA	Nitrate	-11156	-23242
Native NapA	Nitrate	C176D NapA	Nitrate	-12169	-19251
C176D NapA	Nitrate	C176S NapA	Nitrate	1012	-3990
Native NapA	TMAO	C176S NapA	TMAO	-598	-178.4
Native NapA	Nitrate	Native NapA	TMAO	-9557	-19871
C176S NapA	TMAO	C176S NapA	Nitrate	-1000	-3192
C176D NapA	DMSO	C176D NapA	Nitrate	-6927	-261.9

[a]enzyme type and substrate for condition A in equations (1-2), [b]enzyme type and substrate for condition B in equations (1-2), [c]calculated $\Delta\Delta G_b$ values utilizing equation (1) under conditions A and B, [d]calculated $\Delta\Delta G_b^{\ddagger}$ values utilizing equation (2) under conditions A and B.

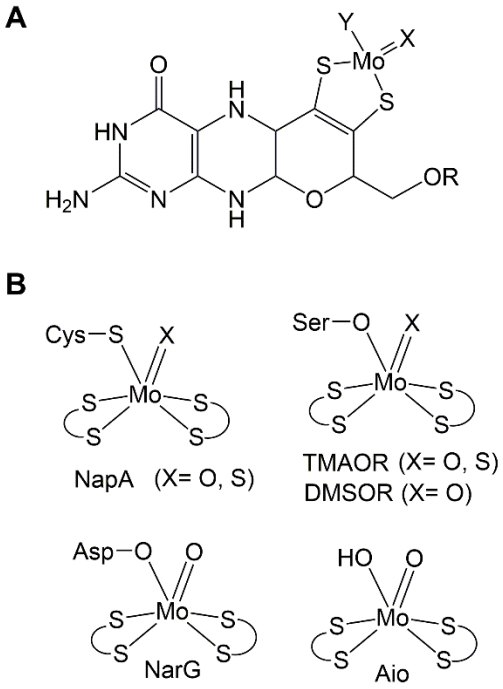

Figure 1: The Molybdenum cofactor (Moco). A) a partial structure of Moco as in Nap, consists of the Mo metal coordinated by two molybdopterin (MPT) molecules (only one is displayed here). The Mo metal is coordinated to four dithiolene sulfurs that are appended to a MPT heterocycle. The generic R group is guanine dinucleotide in Nap. (B) The first coordination sphere of Mo in several members of the DMSOR family.

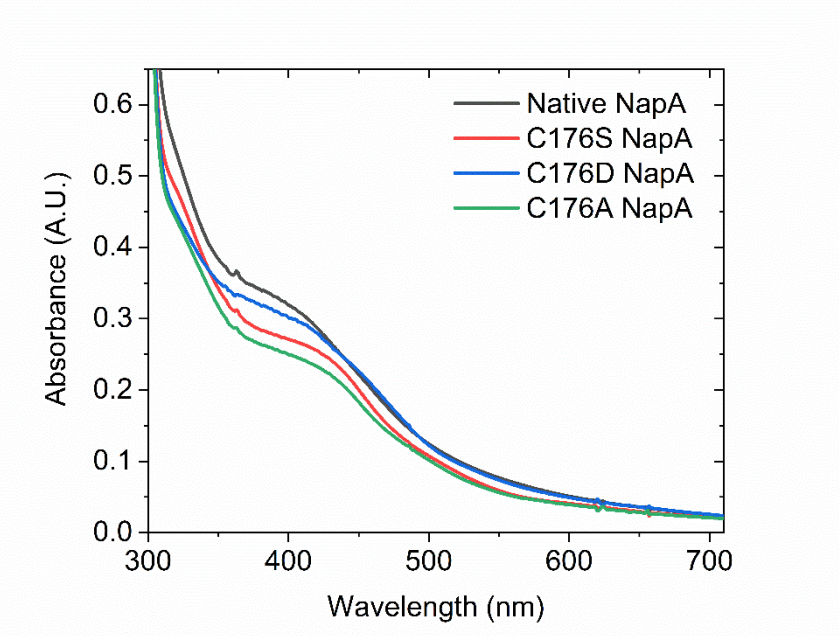

Figure 2: UV-visible spectra of the C176 NapA variants in 50 mM HEPES pH 7.00.

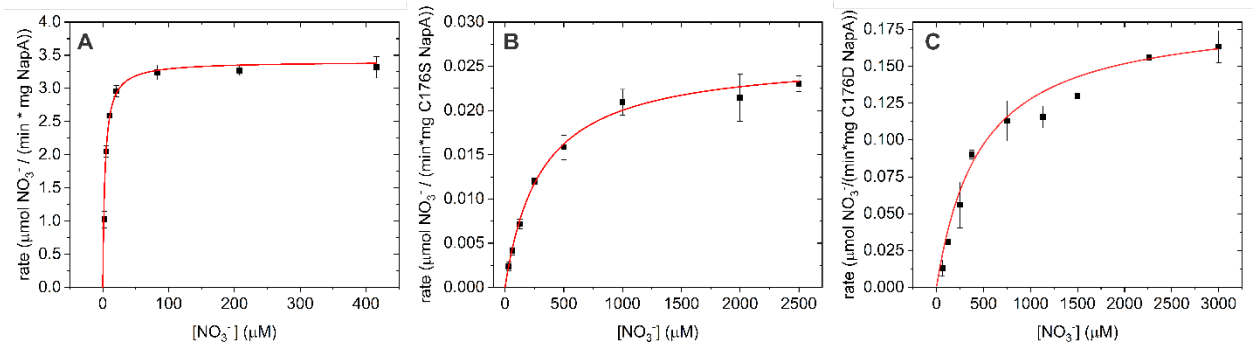

Figure 3: Steady-state kinetic data following the Michaelis Menten model using nitrate as a substrate for (A) native *C. jejuni* NapA (B) C176S *C. jejuni* NapA variant (C) C176D *C. jejuni* NapA variant.

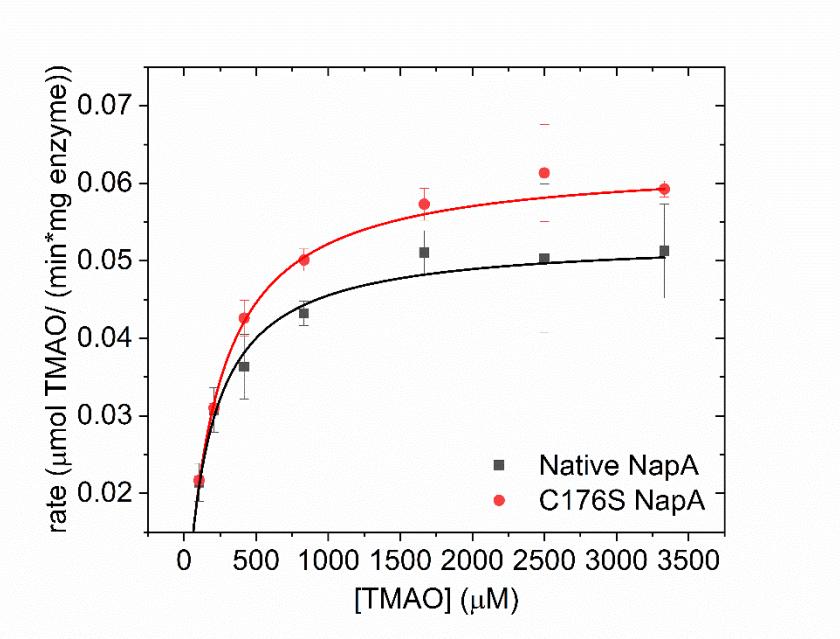

Figure 4: Steady-state kinetic data following the Michaelis Menten model using TMAO as a substrate for native *C. jejuni* NapA (black squares) and C176S NapA (red circles)

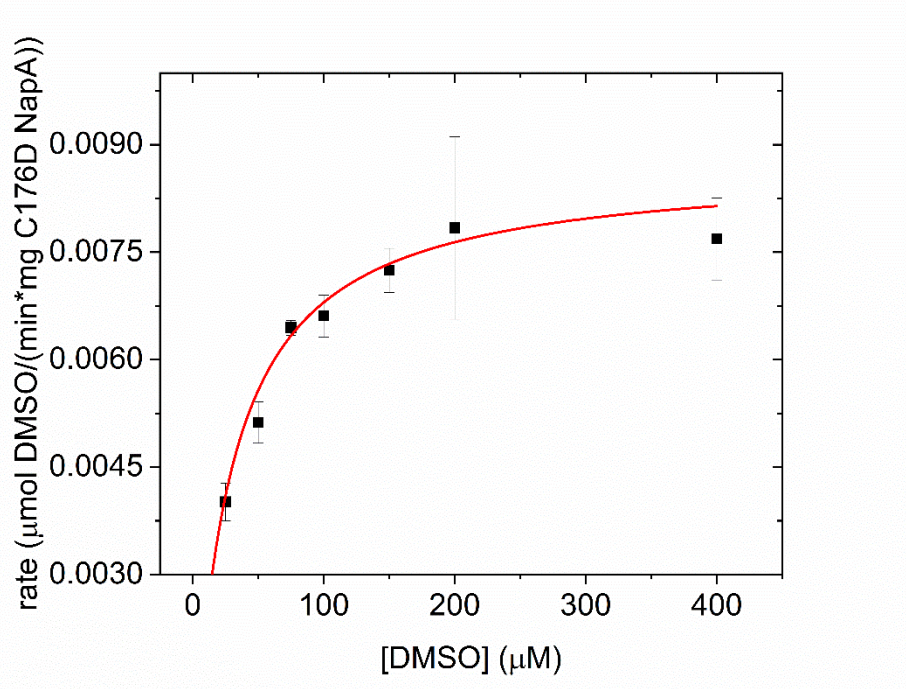

Figure 5: Steady-state kinetic data using DMSO as a substrate for C176D NapA fit to the Michaelis Menten model.

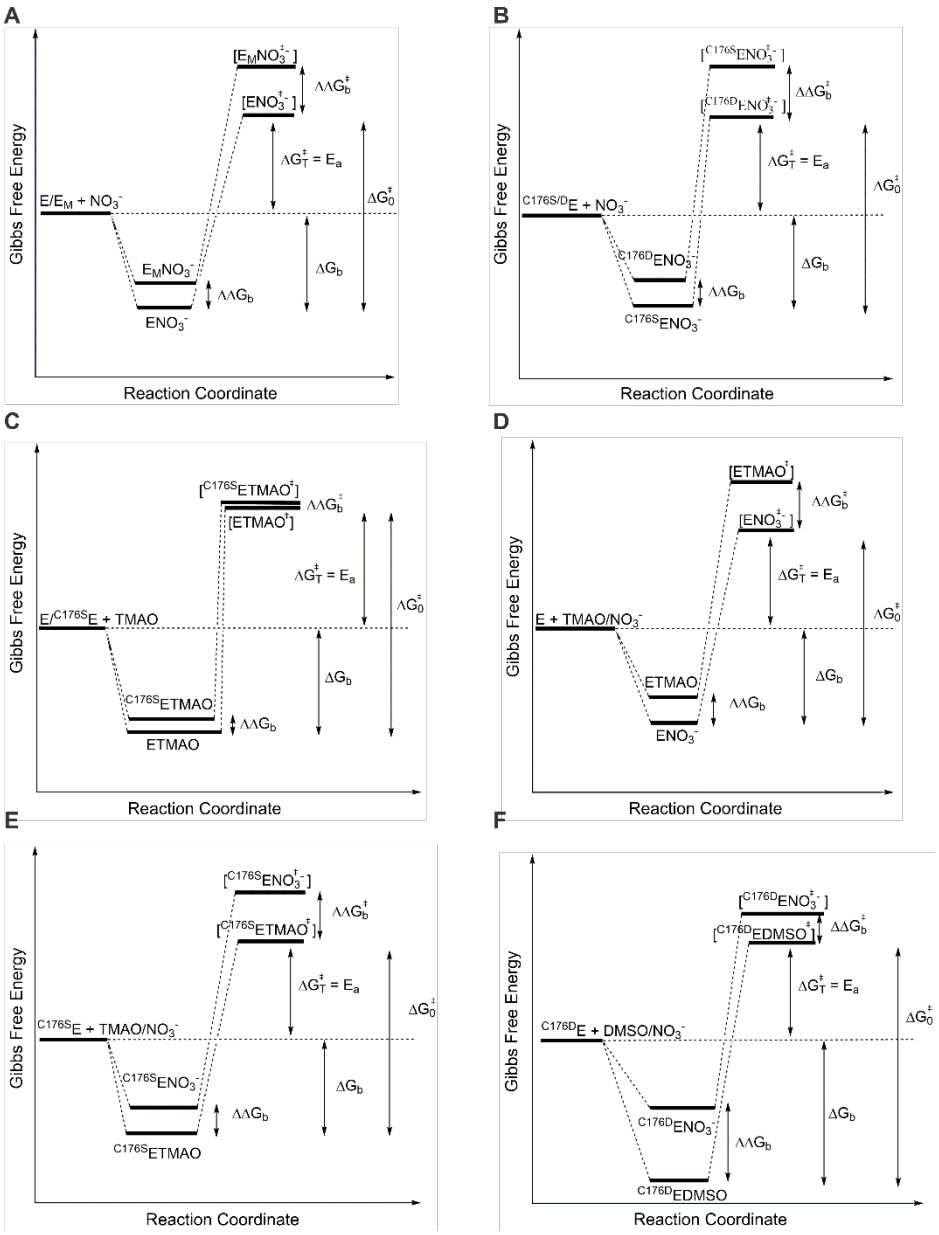

Figure 6: Schematic diagrams depicting energy changes showing the effect of mutation or substrate. The activation energy of nitrate reduction calculated from k_{cat}/K_M is $\Delta G_T^{\ddagger}$ and is composed of two terms: the energetically unfavorable term $\Delta G_0^{\ddagger}$, which represents the activation energy of the chemical steps where bonds are broken and formed (i.e. for k_{cat}), and the energetically favorable term ΔG_b, which represents the realization of binding energy (i.e. from the K_D or estimated from K_M). (A) Diagram comparing the reaction of native NapA enzyme, E, with substrate nitrate to the reaction of C176S/D variant enzymes, E_M, with substrate nitrate. (B) Diagram comparing the reaction of the C176S NapA, ($^{C176S}E$) and C176D NapA ($^{C176D}E$) with substrate nitrate. (C) Diagram comparing the reaction of the E and $^{C176S}E$ with substrate trimethylamine N-oxide (TMAO). (D) Diagram comparing the reaction of the E with substrates nitrate and TMAO. (E) Diagram comparing the reaction of the $^{C176S}E$ with substrates nitrate and TMAO (F) Diagram comparing the reaction of the $^{C176D}E$ with substrates nitrate and dimethyl sulfoxide (DMSO).

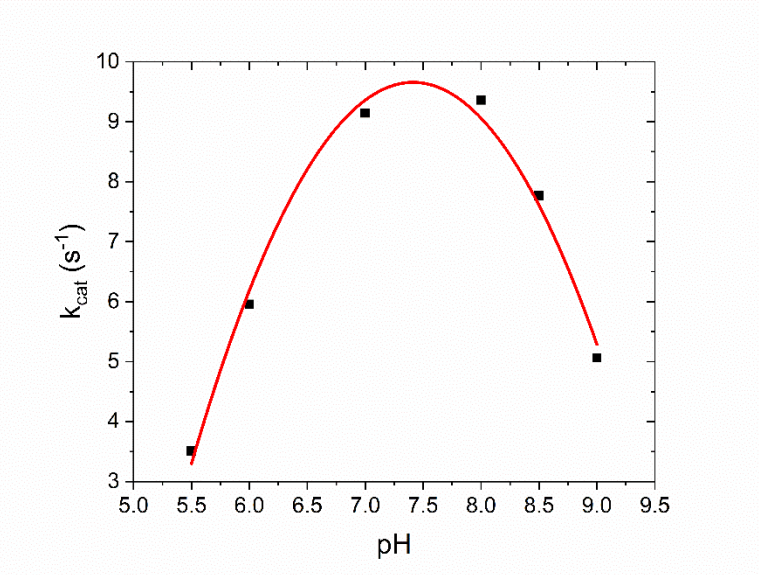

Figure 7: The pH profile for the native *C. jejuni* NapA with nitrate as substrate. NapA pH dependence of k_{cat} with an optimal pH of 7.4.

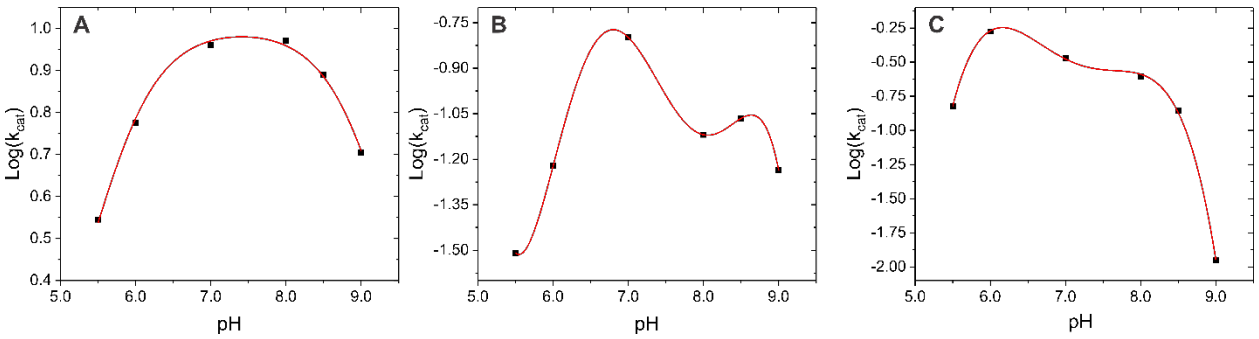

Figure 8: The double logarithmic plot of log(k_{cat}) vs pH for nitrate reduction by A) native NapA, B) C176S NapA, C) C176D NapA represents the pH dependence of the turnover number, k_{cat}, for each of the C176 Nap variants. The data in (A) have been fit to equation (3) in the text and have revealed two catalytically important ionizations in NapA with pK_a of 5.44 and 9.38. The data in (B) and (C) did not converge in the fit to equation (3) and thus have been fit with higher degree polynomials to qualitatively define catalytically important ionizations in the C176S/D variants. Based on the shape of the fitted curve, the C176S/D variants are proposed to form products from multiple protonic states of the ES complex.

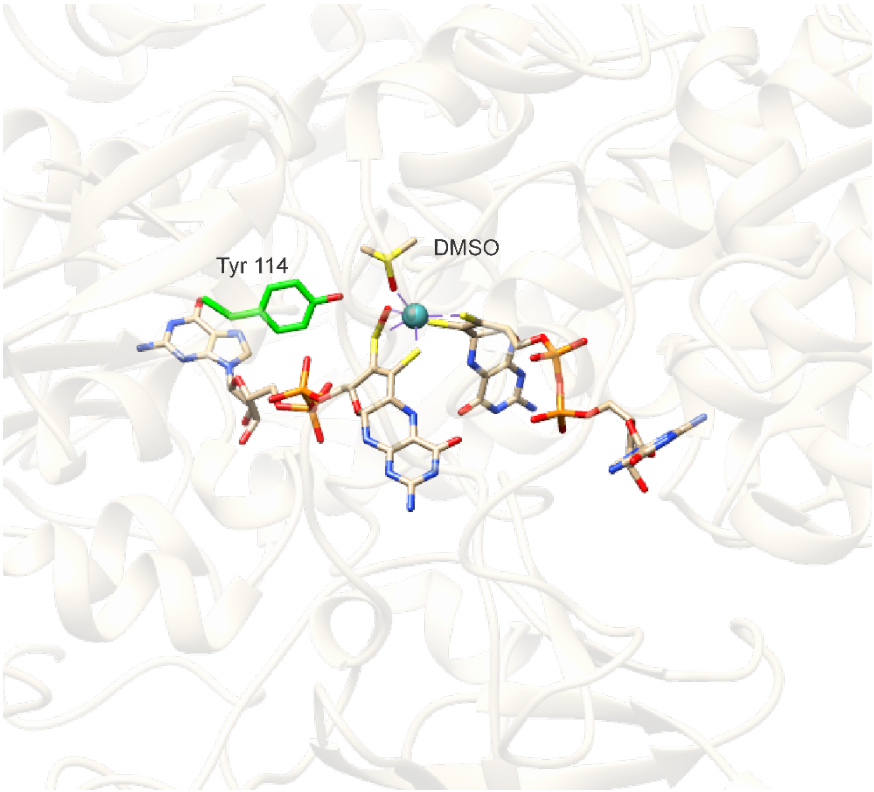

Figure 9: Image of the DMSOR crystal structure (PDB 4DMR) depicting the molybdopterin active site with bound DMSO molecule and Tyr 114 in green.

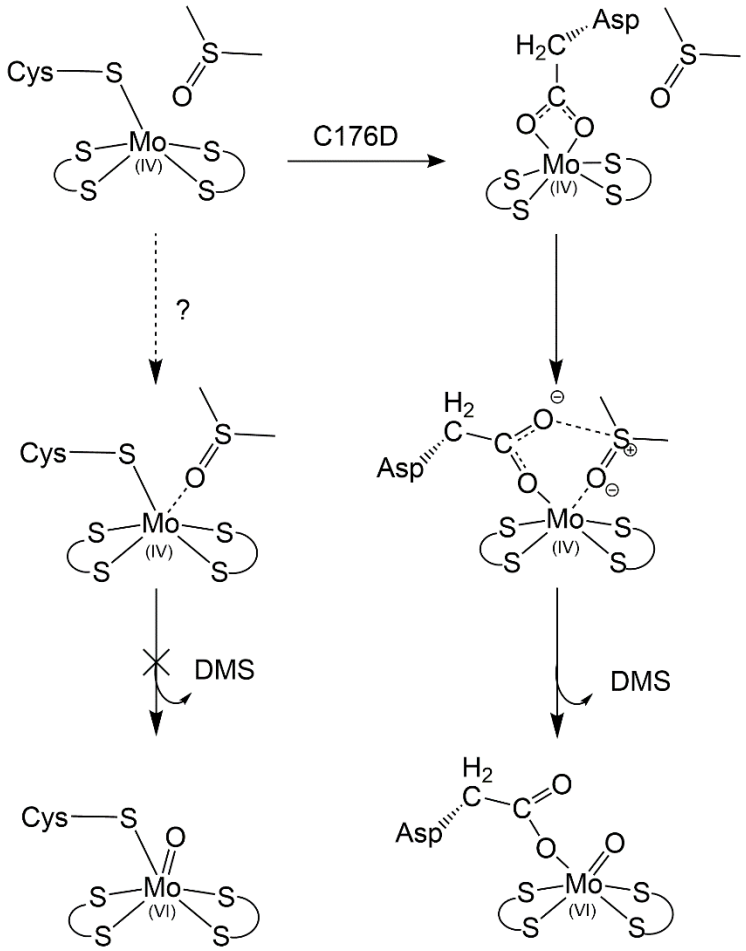

Scheme 1: Proposed interaction of the Asp ligand with bound DMSO compared to a Cys ligand at the active site in NapA variants. The native Nap's interaction with DMSO is shown in the left panel and C176D NapA's interaction is shown in the right panel. It is unclear if DMSO binds in native NapA but DMSO is not turned over. C176D NapA can stabilize DMSO binding to molybdenum through a proposed electrostatic interaction between the partially positive sulfur atom in DMSO and the partially negative carboxylate oxygen atom. The stabilized enzyme-substrate complex in the C176D variant enables DMSO turnover.

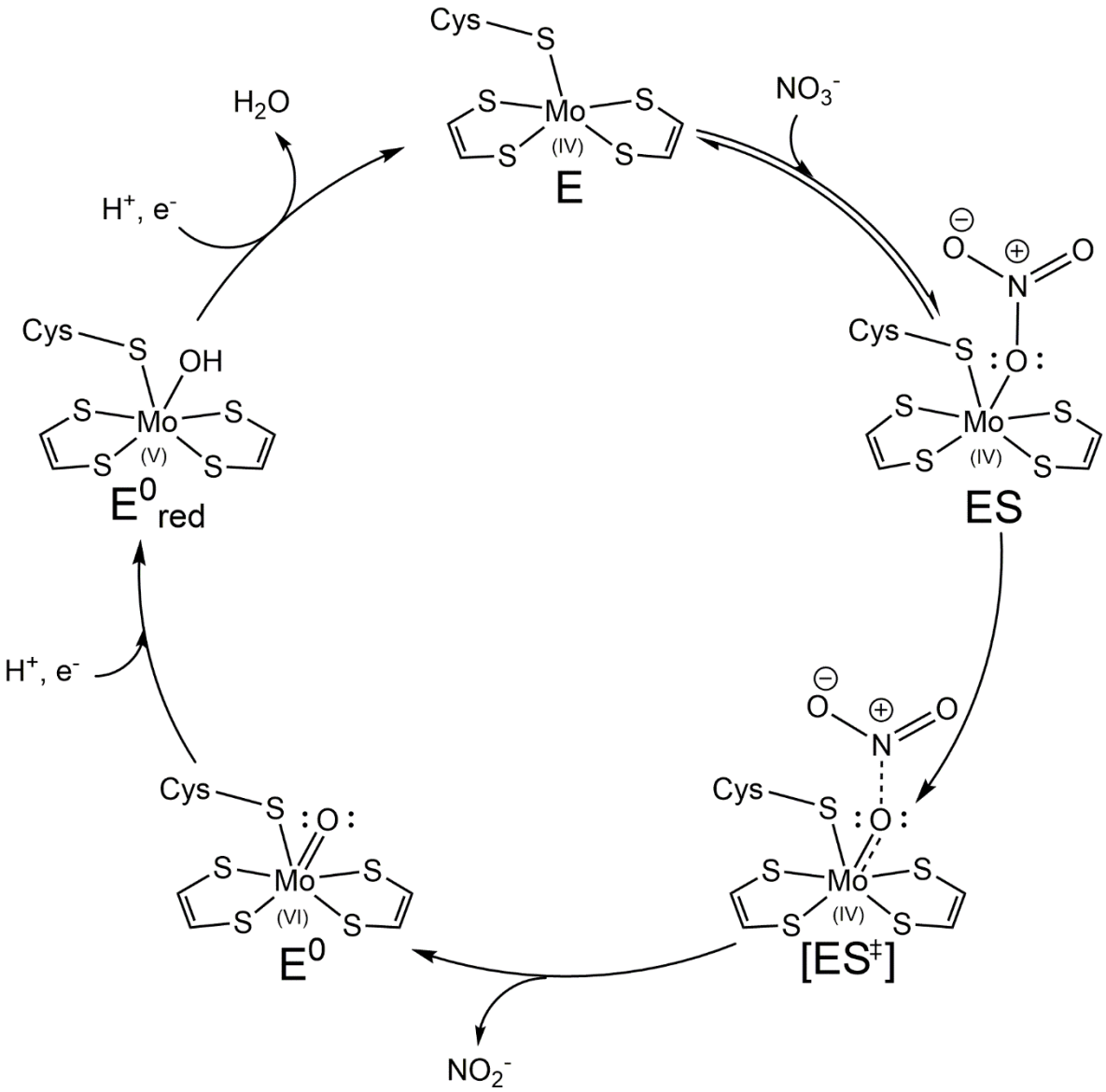

Scheme 2: Catalytic scheme proposal for *C. jejuni* NapA. The reduced molybdenum four state of the enzyme (denoted E) binds reversibly to substrate nitrate (denoted S) in the first step forming the ES complex where nitrate is coordinated to the Mo(IV) metal center. As catalysis proceeds, the O-N bond weakens and the =O bond begins to form in the proposed transition state (denoted [$ES^{\ddagger}$]). Nitrate is reduced to nitrite transferring an oxygen atom to the oxidized Mo(VI) center (denoted E^0). The enzyme is regenerated from the oxidized E^0 state to the fully reduced E state in two proton coupled electron transfer steps with an intermediate Mo(V) state of the enzyme denoted E^0_{red}. The terminal oxo moiety transferred from the original substrate is protonated to produce water. Water diffuses from the active site enabling another substrate molecule to bind to the fully reduced Mo(IV) state (E).

A

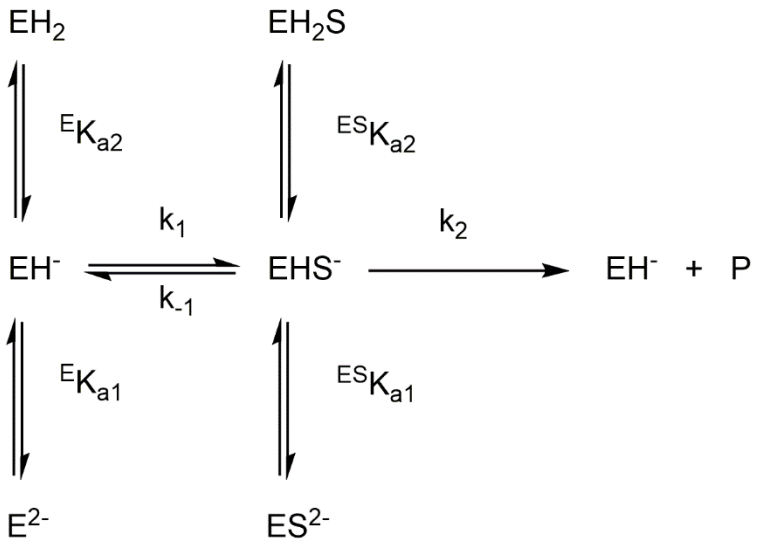

B

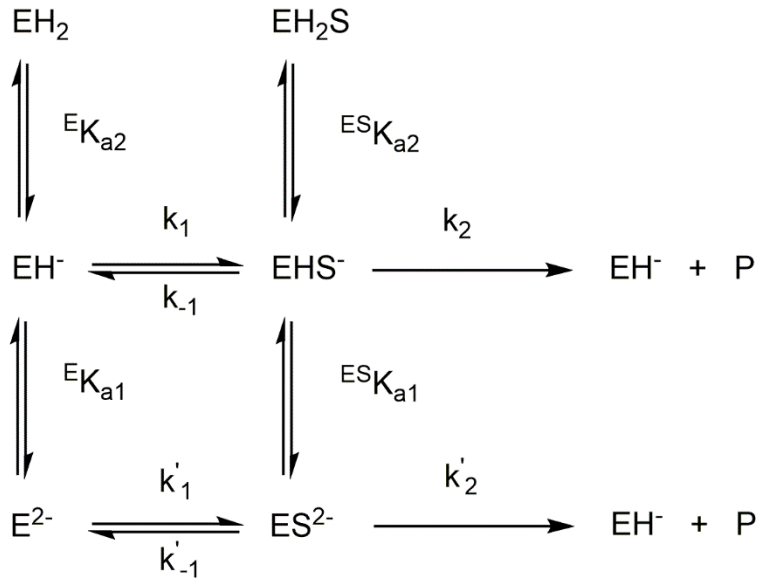

Scheme 3: Proposed protonation states of the NapA enzyme. The free enzyme and enzyme-substrate complex have a simplified form; three protonation forms representing protonation of residues that are catalytically important. The biomolecule can be fully deprotonated, monoprotonated, or diprotonated: A) where only one protonated state, i.e., the monoprotontated state (EHS^-), is catalytically active and B) where two protonic states, i.e. the monoprotonated (EHS^-) and the fully deprotonated (ES^{-2}) states, produce products.

References

1. Schoepp-Cothenet, B., van Lis, R., Philippot, P., Magalon, A., Russell, M. J., and Nitschke, W. (2012) The ineluctable requirement for the trans-iron elements molybdenum and/or tungsten in the origin of life. *Scientific reports* **2**, 263-263
2. Weiss, M. C., Sousa, F. L., Mrnjavac, N., Neukirchen, S., Roettger, M., Nelson-Sathi, S., and Martin, W. F. (2016) The physiology and habitat of the last universal common ancestor. *Nat Microbiol* **1**, 16116
3. Wells, M., Kanmanii, N. J., Al Zadjali, A. M., Janecka, J. E., Basu, P., Oremland, R. S., and Stolz, J. F. (2020) Methane, arsenic, selenium and the origins of the DMSO reductase family. *Sci. Rep.* **10**, 10946
4. Boyington, J. C., Gladyshev, V. N., Khangulov, S. V., Stadtman, T. C., and Sun, P. D. (1997) Crystal structure of formate dehydrogenase H: catalysis involving Mo, molybdopterin, selenocysteine, and an Fe4S4 cluster. *Science* **275**, 1305-1308
5. Mintmier, B., Nassif, S., Stolz, J. F., and Basu, P. (2020) Functional mononuclear molybdenum enzymes: challenges and triumphs in molecular cloning, expression, and isolation. *J Biol Inorg Chem* **25**, 547-569
6. Hettmann, T., Siddiqui, R. A., Frey, C., Santos-Silva, T., Romao, M. J., and Diekmann, S. (2004) Mutagenesis study on amino acids around the molybdenum center of the periplasmic nitrate reductase from *Ralstonia eutropha*. *Biochem. Biophys. Res. Commun.* **320**, 1211-1219
7. Garde, J., Kinghorn, J. R., and Tomsett, A. B. (1995) Site-directed mutagenesis of nitrate reductase from *Aspergillus nidulans*. Identification of some essential and some nonessential amino acids among conserved residues. *J. Biol. Chem.* **270**, 6644-6650
8. Axley, M. J., Boeck, A., and Stadtman, T. C. (1991) Catalytic properties of an *Escherichia coli* formate dehydrogenase mutant in which sulfur replaces selenium. *Proc. Natl. Acad. Sci. U. S. A.* **88**, 8450-8454
9. Pollock, V. V., and Barber, M. J. (2000) Serine 121 is an essential amino acid for biotin sulfoxide reductase functionality. *J. Biol. Chem.* **275**, 35086-35090
10. Schrapers, P., Hartmann, T., Kositzki, R., Dau, H., Reschke, S., Schulzke, C., Leimkuehler, S., and Haumann, M. (2015) Sulfido and cysteine ligation changes at the molybdenum cofactor during substrate conversion by formate dehydrogenase (FDH) from *Rhodobacter capsulatus*. *Inorg. Chem.* **54**, 3260-3271
11. Kaufmann, P., Duffus, B. R., Mitrova, B., Iobbi-Nivol, C., Teutloff, C., Nimtz, M., Jansch, L., Wollenberger, U., and Leimkuhler, S. (2018) Modulating the Molybdenum Coordination Sphere of *Escherichia coli* Trimethylamine N-Oxide Reductase. *Biochemistry* **57**, 1130-1143
12. Trieber, C. A., Rothery, R. A., and Weiner, J. H. (1996) Consequences of removal of a molybdenum ligand (DmsA-Ser-176) of *Escherichia coli* dimethyl sulfoxide reductase. *J. Biol. Chem.* **271**, 27339-27345
13. Hilton, J. C., Temple, C. A., and Rajagopalan, K. V. (1999) Re-design of *Rhodobacter sphaeroides* dimethyl sulfoxide reductase. Enhancement of adenosine N1-oxide reductase activity. *J. Biol. Chem.* **274**, 8428-8436
14. Garrett, R. M., and Rajagopalan, K. V. (1996) Site-directed mutagenesis of recombinant sulfite oxidase. Identification of cysteine 207 as a ligand of molybdenum. *J. Biol. Chem.* **271**, 7387-7391
15. Qiu, J. A., Wilson, H. L., Pushie, M. J., Kisker, C., George, G. N., and Rajagopalan, K. V. (2010) The structures of the C185S and C185A mutants of sulfite oxidase reveal rearrangement of the active site. *Biochemistry* **49**, 3989-4000
16. Reschke, S., Niks, D., Wilson, H., Sigfridsson, K. G. V., Haumann, M., Rajagopalan, K. V., Hille, R., and Leimkuhler, S. (2013) Effect of exchange of the cysteine molybdenum ligand with

selenocysteine on the structure and function of the active site in human sulfite oxidase. *Biochemistry* **52**, 8295-8303
17. Gates, A. J., Richardson, D. J., and Butt, J. N. (2008) Voltammetric characterization of the aerobic energy-dissipating nitrate reductase of *Paracoccus pantotrophus:* exploring the activity of a redox-balancing enzyme as a function of electrochemical potential. *Biochem. J.* **409**, 159-168
18. Sabaty, M., Avazeri, C., Pignol, D., and Vermeglio, A. (2001) Characterization of the reduction of selenate and tellurite by nitrate reductases. *Appl. Environ. Microbiol.* **67**, 5122-5126
19. Johnson, K. E., and Rajagopalan, K. V. (2001) An active site tyrosine influences the ability of the dimethyl sulfoxide reductase family of molybdopterin enzymes to reduce S-oxides. *J. Biol. Chem.* **276**, 13178-13185
20. Morpeth, F. F., and Boxer, D. H. (1985) Kinetic analysis of respiratory nitrate reductase from *Escherichia coli* K12. *Biochemistry* **24**, 40-46
21. Mintmier, B., McGarry, J. M., Sparacino-Watkins, C. E., Sallmen, J., Fischer-Schrader, K., Magalon, A., McCormick, J. R., Stolz, J. F., Schwarz, G., Bain, D. J., and Basu, P. (2018) Molecular cloning, expression and biochemical characterization of periplasmic nitrate reductase from *Campylobacter jejuni*. *FEMS Microbiol Lett* **365**, fny151
22. Fersht, A. (1999) *Structure and Mechanism in Protein Science: A Guide to Enzyme Catalysis and Protein Folding*, W. H. Freeman Company
23. Dixon, M. (1953) The effect of pH on the affinities of enzymes for substrates and inhibitors. *Biochem. J.* **55**, 161-170
24. Tipton, K. F., and Dixon, H. B. F. (1979) Effects of pH on enzymes. *Methods Enzymol.* **63**, 183-234
25. Ellis, P. J., Conrads, T., Hille, R., and Kuhn, P. (2001) Crystal structure of the 100 kDa arsenite oxidase from *Alcaligenes faecalis* in two crystal forms at 1.64 Å and 2.03 Å. *Structure* **9**, 125-132
26. Warelow, T. P., Oke, M., Schoepp-Cothenet, B., Dahl, J. U., Bruselat, N., Sivalingam, G. N., Leimkuehler, S., Thalassinos, K., Kappler, U., Naismith, J. H., and Santini, J. M. (2013) The respiratory arsenite oxidase: structure and the role of residues surrounding the Rieske cluster. *PLoS One* **8**, e72535
27. Bursakov, S., Liu, M.-Y., Payne, W. J., LeGall, J., Moura, I., and Moura, J. J. G. (1995) Isolation and preliminary characterization of a soluble nitrate reductase from the sulfate reducing organism *Desulfovibrio desulfuricans* ATCC 27774. *Anaerobe* **1**, 55-60
28. O'Fagain, C., Butler, B. M., and Mantle, T. J. (1983) The effect of pH on the kinetics of arylsulfatases A and B. *Biochem. J.* **213**, 603-607
29. Brody, M. S., and Hille, R. (1999) The Kinetic Behavior of Chicken Liver Sulfite Oxidase. *Biochemistry* **38**, 6668-6677
30. Cheng, V. W. T., and Weiner, J. H. (2014) S- and N-oxide reductases. *EcoSal Plus*, 1-32
31. Ridge, J. P., Aguey-Zinsou, K.-F., Bernhardt, P. V., Brereton, I. M., Hanson, G. R., and McEwan, A. G. (2002) Site-directed mutagenesis of dimethyl sulfoxide reductase from *Rhodobacter capsulatus*: Characterization of a Y114 → F mutant. *Biochemistry* **41**, 15762-15769
32. Krissinel, E., and Henrick, K. (2004) Secondary-structure matching (SSM), a new tool for fast protein structure alignment in three dimensions. *Acta Crystallogr., Sect. D: Biol. Crystallogr.* **D60**, 2256-2268
33. Fourmond, V., Sabaty, M., Arnoux, P., Bertrand, P., Pignol, D., and Leger, C. (2010) Reassessing the Strategies for Trapping Catalytic Intermediates during Nitrate Reductase Turnover. *J. Phys. Chem. B* **114**, 3341-3347
34. Fourmond, V., Burlat, B., Dementin, S., Sabaty, M., Arnoux, P., Etienne, E., Guigliarelli, B., Bertrand, P., Pignol, D., and Leger, C. (2010) Dependence of Catalytic Activity on Driving Force in Solution Assays and Protein Film Voltammetry: Insights from the Comparison of Nitrate Reductase Mutants. *Biochemistry* **49**, 2424-2432

35. Sadana, J. C., and McElroy, W. D. (1957) Nitrate reductase from *Achromobacter fischeri*. Purification and properties: flavines and cytochrome. *Arch. Biochem. Biophys.* **67**, 16-34
36. Berks, B. C., Richardson, D. J., Robinson, C., Reilly, A., Aplin, R. T., and Ferguson, S. J. (1994) Purification and characterization of the periplasmic nitrate reductase from *Thiosphaera pantotropha*. *Eur. J. Biochem.* **220**, 117-124
37. Bursakov, S. A., Carneiro, C., Almendra, M. J., Duarte, R. O., Caldeira, J., Moura, I., and Moura, J. J. G. (1997) Enzymic properties and effect of ionic strength on periplasmic nitrate reductase (NAP) from *Desulfovibrio desulfuricans* ATCC 27774. *Biochem. Biophys. Res. Commun.* **239**, 816-822
38. Zeamari, K., Gerbaud, G., Grosse, S., Fourmond, V., Chaspoul, F., Biaso, F., Arnoux, P., Sabaty, M., Pignol, D., Guigliarelli, B., and Burlat, B. (2019) Tuning the redox properties of a [4Fe-4S] center to modulate the activity of Mo-bisPGD periplasmic nitrate reductase. *Biochim Biophys Acta Bioenerg* **1860**, 402-413
39. Callister, S. J., Nicora, C. D., Zeng, X., Roh, J. H., Dominguez, M. A., Tavano, C. L., Monroe, M. E., Kaplan, S., Donohue, T. J., Smith, R. D., and Lipton, M. S. (2006) Comparison of aerobic and photosynthetic *Rhodobacter sphaeroides* 2.4.1 proteomes. *J Microbiol Methods* **67**, 424-436
40. John, N., Vidyalakshmi, V. B., and Hatha, A. A. M. (2019) Effect of pH and Salinity on the Production of Extracellular Virulence Factors by *Aeromonas* from Food Sources. *Journal of Food Science* **84**, 2250-2255
41. Do, H., Makthal, N., VanderWal, A. R., Saavedra, M. O., Olsen, R. J., Musser, J. M., and Kumaraswami, M. (2019) Environmental pH and peptide signaling control virulence of *Streptococcus pyogenes* via a quorum-sensing pathway. *Nature Communications* **10**, 2586
42. Israil, A.-M., Delcaru, C., and Balotescu Chifiriuc, M.-C. (2009) Impact of different parameters upon the expression of certain virulence factors of nonhalophilic and halophilic *Vibrio* strains. *Rom. Biotechnol. Lett.* **14**, 4545-4559
43. House, B., Kus, J. V., Prayitno, N., Mair, R., Que, L., Chingcuanco, F., Gannon, V., Cvitkovitch, D. G., and Foster, D. B. (2009) Acid stress-induced changes in enterohemorrhagic *Escherichia coli* O157:H7 virulence. *Microbiology* **155**, 2907-2918
44. De Bernardis, F., Mühlschlegel, F. A., Cassone, A., and Fonzi, W. A. (1998) The pH of the host niche controls gene expression in and virulence of *Candida albicans*. *Infect Immun* **66**, 3317-3325
45. Gates, A. J., Richardson, D. J., and Butt, J. N. (2008) Voltammetric characterization of the aerobic energy-dissipating nitrate reductase of Paracoccus pantotrophus: exploring the activity of a redox-balancing enzyme as a function of electrochemical potential. *Biochem. J.* **409**, 159-168